



UNIVERSITY OF LEEDS

This is a repository copy of *Latitudinal limits to the predicted increase of the peatland carbon sink with warming*.

White Rose Research Online URL for this paper:  
<http://eprints.whiterose.ac.uk/141718/>

Version: Accepted Version

---

**Article:**

Gallego-Sala, AV, Charman, DJ, Brewer, S et al. (72 more authors) (2018) Latitudinal limits to the predicted increase of the peatland carbon sink with warming. *Nature Climate Change*, 8 (10). pp. 907-913. ISSN 1758-678X

<https://doi.org/10.1038/s41558-018-0271-1>

---

© 2018 The Author(s), under exclusive licence to Springer Nature Limited. This is an author produced version of a paper published in *Nature Climate Change*. Uploaded in accordance with the publisher's self-archiving policy.

**Reuse**

Items deposited in White Rose Research Online are protected by copyright, with all rights reserved unless indicated otherwise. They may be downloaded and/or printed for private study, or other acts as permitted by national copyright laws. The publisher or other rights holders may allow further reproduction and re-use of the full text version. This is indicated by the licence information on the White Rose Research Online record for the item.

**Takedown**

If you consider content in White Rose Research Online to be in breach of UK law, please notify us by emailing [eprints@whiterose.ac.uk](mailto:eprints@whiterose.ac.uk) including the URL of the record and the reason for the withdrawal request.



[eprints@whiterose.ac.uk](mailto:eprints@whiterose.ac.uk)  
<https://eprints.whiterose.ac.uk/>

# 1 Latitudinal limits to the predicted increase of the peatland carbon sink with warming

2  
3 Angela V. Gallego-Sala<sup>1\*</sup>, Dan J. Charman<sup>1\*</sup>, Simon Brewer<sup>2</sup>, Susan E. Page<sup>3</sup>, I. Colin Prentice<sup>4</sup>,  
4 Pierre Friedlingstein<sup>5</sup>, Steve Moreton<sup>6</sup>, Matthew J. Amesbury<sup>1</sup>, David W. Beilman<sup>7</sup>, Svante Björck<sup>8</sup>,  
5 Tatiana Blyakharchuk<sup>9</sup>, Christopher Bochicchio<sup>10</sup>, Robert K. Booth<sup>10</sup>, Joan Bunbury<sup>11</sup>, Philip  
6 Camill<sup>12</sup>, Donna Carless<sup>1</sup>, Rodney A. Chimner<sup>13</sup>, Michael Clifford<sup>14</sup>, Elizabeth Cressey<sup>1</sup>, Colin  
7 Courtney-Mustaphi<sup>15,16</sup>, François De Vleeschouwer<sup>17</sup>, Rixt de Jong<sup>8</sup>, Barbara Fialkiewicz-Koziel<sup>18</sup>,  
8 Sarah A. Finkelstein<sup>19</sup>, Michelle Garneau<sup>20</sup>, Esther Githumbi<sup>15</sup>, John Hribljan<sup>13</sup>, James Holmquist<sup>21</sup>,  
9 Paul D. M. Hughes<sup>22</sup>, Chris Jones<sup>23</sup>, Miriam C. Jones<sup>24</sup>, Edgar Karofeld<sup>25</sup>, Eric S. Klein<sup>26</sup>, Ulla  
10 Kokfelt<sup>8</sup>, Atte Korhola<sup>27</sup>, Terri Lacourse<sup>28</sup>, Gael Le Roux<sup>17</sup>, Mariusz Lamentowicz<sup>18,29</sup>, David Large<sup>30</sup>,  
11 Martin Lavoie<sup>31</sup>, Julie Loisel<sup>32</sup>, Helen Mackay<sup>33</sup>, Glen M. MacDonald<sup>21</sup>, Markku Makila<sup>34</sup>, Gabriel  
12 Magnan<sup>20</sup>, Robert Marchant<sup>15</sup>, Katarzyna Marcisz<sup>18,29,35</sup>, Antonio Martínez Cortizas<sup>36</sup>, Charly Massa<sup>7</sup>,  
13 Paul Mathijssen<sup>27</sup>, Dmitri Mauquoy<sup>37</sup>, Timothy Mighall<sup>37</sup>, Fraser J.G. Mitchell<sup>38</sup>, Patrick Moss<sup>39</sup>,  
14 Jonathan Nichols<sup>40</sup>, Pirta O. Oksanen<sup>41</sup>, Lisa Orme<sup>1,42</sup>, Maara S. Packalen<sup>43</sup>, Stephen Robinson<sup>44</sup>,  
15 Thomas P. Roland<sup>1</sup>, Nicole K. Sanderson<sup>1</sup>, A. Britta K. Sannel<sup>45</sup>, Noemí Silva-Sánchez<sup>36</sup>, Natascha  
16 Steinberg<sup>1</sup>, Graeme T. Swindles<sup>46</sup>, T. Edward Turner<sup>46,47</sup>, Joanna Uglow<sup>1</sup>, Minna Väliranta<sup>27</sup>, Simon  
17 van Bellen<sup>20</sup>, Marjolein van der Linden<sup>48</sup>, Bas van Geel<sup>49</sup>, Guoping Wang<sup>50</sup>, Zicheng Yu<sup>10,51</sup>, Joana  
18 Zaragoza-Castells<sup>1</sup>, Yan Zhao<sup>52</sup>

19  
20 \*Authors for correspondence

21 <sup>1</sup>Geography Department, Amory Building, Rennes Drive, University of Exeter, Exeter, EX4 4RJ, United Kingdom

22 <sup>2</sup>Department of Geography, University of Utah, Salt Lake City, UT, USA

23 <sup>3</sup>School of Geography, Geology and the Environment, University of Leicester, Leicester, UK

24 <sup>4</sup>AXA Chair of Biosphere and Climate Impacts, Department of Life Sciences, Imperial College London, Silwood Park, Ascot, UK

25 <sup>5</sup>College of Engineering, Maths and Physics, University of Exeter, Exeter, UK

26 <sup>6</sup>NERC Radiocarbon Facility, East Kilbride, UK

27 <sup>7</sup>Department of Geography, University of Hawaii at Manoa, Honolulu, HI, USA

28 <sup>8</sup>Department of Geology, Lund University, Lund, Sweden

29 <sup>9</sup>Institute for Monitoring Climatic & Ecological Systems, Siberian branch of the Russian Academy of Science (IMCES SB RAS), Tomsk, Russia

30 <sup>10</sup>Department of Earth and Environmental Science, Lehigh University, Bethlehem, PA, USA

31 <sup>11</sup>Department of Geography and Earth Science, University of Wisconsin-La Crosse, La Crosse, WI, US

32 <sup>12</sup>Environmental Studies Program and Earth and Oceanographic Science Department, Bowdoin College, Brunswick, ME, USA

33 <sup>13</sup>School of Forest Research and Environmental Sciences, Michigan Technical University, Houghton, MI, USA

34 <sup>14</sup>DRI, Division of Earth and Ecosystem Science, Las Vegas, NV, USA

35 <sup>15</sup>Environment Department, University of York, York, UK

36 <sup>16</sup>Department of Archaeology and Ancient History, Uppsala Universitet, Uppsala, Sweden

37 <sup>17</sup>EcoLab, Université de Toulouse, CNRS, INPT, UPS, Castanet Tolosan, France

38 <sup>18</sup>Department of Biogeography & Palaeoecology, Adam Mickiewicz University, Poznań, Poland

39 <sup>19</sup>Department of Earth Sciences, University of Toronto, Toronto, Canada

40 <sup>20</sup>GEOTOP, Université du Québec à Montréal, Canada

41 <sup>21</sup>Institute of Environment & Sustainability, University of California Los Angeles, Los Angeles, CA, USA

42 <sup>22</sup>Geography and Environment, University of Southampton, Southampton, UK

43 <sup>23</sup>MET Office, Hadley Centre, Exeter, UK

44 <sup>24</sup>USGS, Reston, Virginia, VA, USA

45 <sup>25</sup>Institute of Ecology & Earth Sciences, University of Tartu, Tartu, Estonia

46 <sup>26</sup>Department of Geological Sciences, University of Alaska Anchorage, Anchorage, AK, USA

47 <sup>27</sup>ECRU, University of Helsinki, Helsinki, Finland

48 <sup>28</sup>Department of Biology and Centre for Forest Biology, University of Victoria, Victoria, Canada

49 <sup>29</sup>Laboratory of Wetland Ecology & Monitoring, Adam Mickiewicz University, Poznań, Poland

50 <sup>30</sup>Department Of Chemical and Environmental Engineering, University of Nottingham, Nottingham, UK

51 <sup>31</sup>Département de Géographie & Centre d'Études Nordiques, Université Laval, Québec City, Canada

52 <sup>32</sup>Department of Geography, Texas A&M University, College Station, TX, USA

53 <sup>33</sup>School of Geography, Politics and Sociology, Newcastle University, Newcastle, UK

54 <sup>34</sup>Geological Survey of Finland, Espoo, Finland

55 <sup>35</sup>Institute of Plant Sciences & Oeschger Centre for Climate Change Research, University of Bern, Bern, Switzerland

56 <sup>36</sup>Departamento de Edafología e Química Agrícola, Universidade de Santiago de Compostela, Spain

57 <sup>37</sup>Geosciences, University of Aberdeen, Aberdeen, UK

58 <sup>38</sup>School of Natural Sciences, Trinity College Dublin, Dublin, Ireland

59 <sup>39</sup>School of Earth and Environmental Sciences, The University of Queensland, Brisbane, Australia

60 <sup>40</sup>Lamont-Doherty Earth Observatory, Columbia University, Palisades, NY, USA

61 <sup>41</sup>Previously at the Arctic Centre, University of Lapland, Rovaniemi, Finland

62 <sup>42</sup>Department of Geology and Geophysics, Norwegian Polar Institute, Tromsø, Norway

63 <sup>43</sup>Science and Research Branch, Ministry of Natural Resources and Forestry, Sault Ste. Marie, Canada

64 <sup>44</sup>Champlain College, Dublin, Ireland

65 <sup>45</sup>Department of Physical Geography, Stockholm University, Stockholm, Sweden

66 <sup>46</sup>School of Geography, University of Leeds, Leeds, UK

67 <sup>47</sup>The Forestry Commission, Galloway Forest District, Scotland, UK

68

69  
70  
71  
72  
73  
74

<sup>48</sup>BIAAX Consult, Zaandam, The Netherlands

<sup>49</sup>IBED, Universiteit van Amsterdam, Amsterdam, The Netherlands

<sup>50</sup>Northeast Institute of Geography & Agroecology, Chinese Academy of Science, Changchun, China

<sup>51</sup>Key Laboratory of Wetland Ecology, Institute for Mire and Peat Research, Northeast Normal University, Changchun, China

<sup>52</sup>Institute of Geographical Science & Natural Resources, Chinese Academy of Science, Beijing, China

75  
76  
77

Key words: peatlands, carbon cycle, climate change, tropical peat, last millennium.

78  
79  
80  
81  
82  
83  
84  
85  
86  
87  
88  
89  
90  
91

**The carbon sink potential of peatlands depends on the balance between carbon uptake by plants and microbial decomposition. The rates of both these processes will increase with warming but it remains unclear which will dominate the global peatland response. Here we examine the global relationship between peatland carbon accumulation rates during the last millennium and planetary-scale climate space. A positive relationship is found between carbon accumulation and cumulative photosynthetically active radiation during the growing season for mid- to high-latitude peatlands in both hemispheres. However, this relationship reverses at lower latitudes, suggesting that carbon accumulation is lower under the warmest climate regimes. Projections under RCP2.6 and RCP8.5 scenarios indicate that the present-day global sink will increase slightly until ~2100 AD but decline thereafter. Peatlands will remain a carbon sink in the future, but their response to warming switches from a negative to a positive climate feedback (decreased carbon sink with warming) at the end of the 21st century.**

92  
93  
94  
95  
96  
97  
98

---

Analysis of peatland carbon accumulation over the last millennium and its association with global-scale climate space indicates an ongoing carbon sink into the future, but with decreasing strength as conditions warm.

---

99  
100  
101  
102  
103  
104  
105  
106  
107

The carbon cycle and the climate form a feedback loop and coupled carbon cycle climate model simulation results show that this feedback is positive<sup>1</sup>. In simple terms, warming of the Earth's surface results in a larger fraction of the anthropogenically and naturally released CO<sub>2</sub> remaining in the atmosphere, inducing further warming. However, the strength of this feedback is highly uncertain; indeed, it is now one of the largest uncertainties in future climate predictions<sup>2</sup>. The terrestrial carbon cycle feedback is potentially larger in magnitude when compared to the ocean carbon cycle feedback, and it is also the more poorly quantified<sup>1,3</sup>. In coupled climate models, there is still no consensus on the overall sensitivity of the land processes, or whether changes in net primary productivity versus changes in

108 respiration will dominate the response<sup>1</sup>. Furthermore, most models have so far ignored the  
109 potential contribution of peatlands, even though they contain 530-694 Gt C<sup>1,4</sup>; equalling the  
110 amount of carbon in the pre-industrial atmosphere. The few models that have taken into  
111 account the role of peatlands in the carbon cycle predict a sustained carbon sink (global  
112 dynamic vegetation models<sup>5,6</sup>) or a loss of sink potential in the future (soil decomposition  
113 model<sup>7</sup>) depending on the climate trajectories and the specific model<sup>5,6,7</sup>.

114 Evidence from field manipulation experiments suggests major future carbon losses from  
115 increased respiration in peatlands with warming<sup>8</sup>, but these projections do not take into account  
116 the potential increased productivity due to increased temperatures and growing season length,  
117 especially in mid- to high-latitude peatlands. Additionally, increased loss of carbon due to  
118 warming may be limited to the upper layers of peat but it may not affect the buried deeper  
119 anoxic layers<sup>9,10</sup>.

120 Peatlands preserve a stratigraphic record of net carbon accumulation, the net outcome of both  
121 respiration and plant production, and these records can be used to examine the behaviour of  
122 the peatland sink over time. This has been done successfully since the last deglaciation (11,700  
123 years ago to the present) at lower resolution<sup>4,11</sup> and for the last millennium (850-1850 AD) at  
124 higher temporal resolution<sup>12</sup>. These studies have focused on high latitude northern peatlands  
125 and have shown that in warmer climates increases in plant productivity overcome increases in  
126 respiration and that these peatlands will likely become a more efficient sink if soil moisture is  
127 maintained<sup>11,12,13</sup>.

128 Here we use 294 profiles from globally distributed peatlands to build a dataset of global carbon  
129 accumulation over the last millennium (850-1850 AD) (Figure 1a). We improve the coverage  
130 of northern high latitudes and expand the dataset to low latitudes and southern high latitudes  
131 by including over 200 new profiles compared to previous data compilations<sup>12</sup>. There are areas  
132 of the world where extensive peatlands exist where data are still lacking (e.g. East Siberia,  
133 Congo Basin<sup>14</sup>), but our data provide comprehensive coverage of peatland carbon accumulation  
134 records over this time period. The last millennium is chosen as a time span because it is  
135 climatically relatively similar to the present day enabling comparisons with modern planetary-  
136 scale climate space, it is possible to date this part of the peat profile accurately, and the data  
137 density is greatest for this period as almost all existing peatlands contain peat from this time.

138 **Planetary-scale climate effects on the carbon sink**

139 The profiles are predominantly from low nutrient sites (213 sites, Fig 1b), and the spatial  
140 patterns of the distribution show that oceanic peatlands tend to be characterised by low  
141 nutrients (bogs) while there are continental areas (e.g. central Asia, North America, Arctic  
142 Eurasia) where there are extensive higher nutrient peatlands (fens, including poor fens).  
143 Mean carbon accumulation rates for the last millennium vary between 3 and 80 g C m<sup>-2</sup> yr<sup>-1</sup>  
144 (see Methods, and Figure 1c).

145

146 Photosynthetically active radiation summed over the growing season (PAR0) is the best  
147 explanatory variable of all of the bioclimatic variables that were statistically fitted to carbon  
148 accumulation (Figure 2a), in agreement with a previous study of northern peatlands<sup>12</sup>. Carbon  
149 accumulation increases almost linearly with increasing PAR0 up to PAR0 values of around  
150 8000 mol phot m<sup>-2</sup>, which correspond to peatland sites in the mid-latitudes, including those  
151 from the Southern Hemisphere. The positive relationship for PAR0 is spatially explicit at  
152 these mid- to high latitudes, with temperate sites accumulating more carbon than boreal or  
153 arctic areas (Figure 1c). The positive relationship peaks at values of PAR0 ~ 8000 mol phot  
154 m<sup>-2</sup> (8000 mol phot m<sup>-2</sup> for bogs and 10,000 mol phot m<sup>-2</sup> for fens), representing sites from  
155 mid latitudes, and appears to reverse when PAR0 >11,000 mol phot m<sup>-2</sup>, values which  
156 represent the tropical sites (Figure 2b). The growing season length at mid latitude locations is  
157 at or very close to 365 days a year, so further warming no longer extends the length of the  
158 growing season at these sites. The relationship is similar but weaker for growing degree days  
159 (GDD0, Figure 2c) and growing season length (GSL, Figure SI1c), suggesting that increased  
160 accumulation is primarily driven by growing season length, and partly by light availability.

161

162 For the lower latitude peatlands, we suggest that the higher temperatures drive increased  
163 microbial activity and decomposition rates in the peat and surface litter, but this is not fully  
164 compensated by increases in plant productivity (Figure SI4), leading to reduced carbon  
165 accumulation rates compared to higher latitude peatlands. It has been shown that plant  
166 productivity does not increase with temperature after accounting for the increased length of  
167 the growing season<sup>15</sup>. This has important implications in terms of the future carbon sink. Our  
168 results suggest that under a future warmer climate, the increase in net primary productivity,  
169 due to longer and warmer growing seasons, results in more carbon accumulation only at mid-  
170 to high-latitudes. Conversely, increased respiration dominates the response of peatlands to  
171 warming at lower latitudes, even if this warming is predicted to be less compared to the more  
172 amplified warming at high latitudes. Thus, the carbon sink of low latitude peatlands will

173 decrease with warmer temperatures, although uncertainty in the carbon accumulation trend  
174 for low latitudes is higher, due to the more limited extent of data for these areas. Furthermore,  
175 the greater predictive power of PAR0 suggests that light availability is a critical factor in  
176 driving the increase in net primary productivity at higher latitudes, in agreement with  
177 previous theoretical analysis of plant photosynthesis<sup>16</sup>. Cloud cover and PAR0 remain highly  
178 uncertain in future climate projections, and this needs to be considered in estimates of the  
179 precise effect of future climate change on peatland carbon accumulation rates.

180

181 We expected moisture to be an important controlling variable for carbon accumulation.  
182 However, the effect of moisture was not detected using a moisture index (Figure 2d) and  
183 instead the relationship between moisture index and carbon accumulation indicates that  
184 moisture acts as an on-off switch, i.e. there needs to be sufficient moisture to retard decay but  
185 increases to very high moisture levels do not promote higher rates of accumulation. A  
186 precipitation deficit analysis was also carried out (Figure SI5) to ascertain whether a greater  
187 precipitation shortage drives reduced carbon accumulation, but there are no clear patterns  
188 emerging using this moisture parameter either. None of the moisture indexes used account for  
189 local small-scale hydrological or water chemistry variations. Because our data does not  
190 support a moisture control on global-scale variations in vertical peat accumulation, we have  
191 not used moisture as a predictor variable in our future estimates of the carbon sink.

192

### 193 **The present and future of the carbon sink**

194 We estimated the total present and future global peatland carbon sink strength using both  
195 spatially interpolated observations and statistically modelled data (see methods). According  
196 to the spatially interpolated observations (Figure 3a) of last millennium carbon accumulation  
197 rates, global peatlands represent an average apparent carbon sink of  $142 \pm 7 \text{ Tg C yr}^{-1}$  over the  
198 last millennium. This is equivalent to a total millennial sink of  $33 \pm 2 \text{ ppm CO}_2$ , based on a  
199 simple conversion from change in carbon pool to atmospheric  $\text{CO}_2$  of  $2.123 \text{ GtC} = 1 \text{ ppm}$  and  
200 an airborne fraction of 50 % to account for the carbon cycle response to any carbon dioxide  
201 released to or captured from the atmosphere<sup>17</sup>. This figure corresponds to the near-natural  
202 sink and does not account for anthropogenic impacts such as land use change, drainage or  
203 fires, and also excludes the very slow decomposition that continues in the deeper anoxic  
204 layers of peat older than 1000 years.

205 There are few directly comparable estimates of the total peatland sink, but a simplistic

206 estimate based on a series of assumptions of average peat depth, extent and bulk density  
207 suggested a current rate of 96 Tg C yr<sup>-1</sup> for northern peatlands alone<sup>15</sup>. A subsequent estimate  
208 suggests a figure of approximately 110 Tg C yr<sup>-1</sup> global peatland net carbon uptake for the  
209 last 1000 years<sup>4</sup> (see Figure 5 in ref. 4), with 90 Tg C yr<sup>-1</sup> in northern peatlands. These  
210 estimates are based on averages across very large regions. Our spatially explicit modelling  
211 suggests a larger overall carbon sink than these earlier estimates and implies that the size of  
212 the global peatland carbon sink is substantially larger than previously thought. This is also a  
213 larger value than estimates of the average carbon accumulation rates over the entire Holocene  
214 (>50 to 96 Tg C yr<sup>-1</sup>)<sup>4,18</sup>, principally because the total area of peatlands is at its greatest in the  
215 last millennium when compared with the earlier in the Holocene. In addition, many high  
216 latitude peatlands only accumulated small amounts of peat during the early stages  
217 (minerotrophic) of their development, often for several millennia after their initiation<sup>19,20</sup>.

218

219 None of the above estimates take into account the long-term decay of previously deposited  
220 deeper/older peat. Prior estimates<sup>4</sup> (Figure 5 in ref. 4) suggest that this loss is substantial at  
221 around 65 Tg C yr<sup>-1</sup>, producing a net carbon balance of around 45 Tg C yr<sup>-1</sup> compared to a  
222 net uptake value of 110 Tg C yr<sup>-1</sup> in the same study. For northern peatlands alone, an earlier  
223 estimate of the deep carbon loss<sup>4</sup> was approximately less than half of the equivalent later  
224 estimate<sup>9</sup> for the same region, c. 48 Tg C yr<sup>-1</sup>. However, all of these estimates are based on  
225 modelling using a ‘super-peatland’ approach combining data from across large areas to  
226 estimate mean long term peat decay rates and thus are subject to considerable error.  
227 Nevertheless, the net carbon balance including the decay of deeper/older peat is likely to be  
228 around a third less than our 142±7 Tg C yr<sup>-1</sup> estimate of the apparent global net uptake over  
229 the last millennium, assuming a long-term decay rate between 20 and 50 Tg C yr<sup>-1</sup>.

230

231 Modelled changes in the future peatland carbon sink under a warmer climate show a slight  
232 increase in the global peatland sink compared to the present-day sink until 2100 AD (RCP  
233 2.6 scenario: 147 ± 7 Tg C yr<sup>-1</sup>; RCP 8.5 scenario: 149± 7 Tg C yr<sup>-1</sup>) and a decrease in the  
234 sink thereafter (Figure SI3, Table SI3). The results suggest that initially, and approximately  
235 for the next century, peatlands will be a small negative feedback to climate change, i.e. the  
236 global peatland carbon sink increases as it gets warmer. However, this negative feedback  
237 does not persist in time and the strength of the sink starts to decline again after 2100 AD,  
238 although it remains above the 1961-1990 values throughout the next c.300 years (RCP 2.6

239 scenario:  $146 \pm 7 \text{ Tg C yr}^{-1}$ ; RCP 8.5 scenario:  $145 \pm 7 \text{ Tg C yr}^{-1}$  for the period 2080-2300).  
240 Despite large uncertainties in these projections due to uncertainties originating from both the  
241 statistical modelling and from the climate model projections, the direction of change and a  
242 shift from initially negative to subsequent positive feedback is a plausible and robust result.  
243

244 An explanation for the mechanism of change in the sink capacity of the global peatland area  
245 can be inferred from the spatial distribution of the modelled changes (Figure 4). While the  
246 carbon sink at very high latitudes increases in both RCP2.6 and RCP8.5 scenarios  
247 continuously to 2300 AD, the lower latitudes experience an ongoing decrease in carbon  
248 sequestration over the same period. Simultaneously, peatlands in the mid latitudes gradually  
249 move past the optimum level of photosynthesis/respiration into the decline phase (Figure 2a,  
250 Figure SI4) where respiratory losses are rising faster than net primary productivity. This is  
251 likely to be determined by the poleward migration of the latitudinal line where the growing  
252 season length is near 365 days, moderated by changes in cloud cover and thus PAR. The  
253 balance between the increasing high latitude sink, and the decreasing low latitude sink  
254 changes over time, such that the global sink eventually begins to decrease. This estimate  
255 takes into account only the changes in the surface accumulation rates of extant peatlands and  
256 other factors will affect the total peatland carbon balance. Deeper peat may also warm and  
257 provide a further source of peatland carbon release in peatlands worldwide, but there is still  
258 some debate as to how large this effect may be, especially in the transition from permafrost to  
259 unfrozen peatlands<sup>21,22</sup>

260 Conversely, peatlands may expand into new areas that have previously been too cold or too  
261 dry for substantial soil carbon accumulation especially in northern high latitudes, where there  
262 are large topographically suitable land areas. The magnitude of these potential changes is  
263 unknown, but it would offset at least some of the additional loss of carbon from enhanced  
264 deep peat decay. Carbon dioxide fertilization is also likely to increase the peatland carbon  
265 sink via increases in primary productivity. Furthermore, vegetation changes and specifically  
266 more woody vegetation might result in a larger peatland sink, if moisture is maintained<sup>23</sup>.  
267 Increases in shrubs and trees have also been shown to increase the pools of phenolic  
268 compounds and decrease the losses of peat carbon to the atmosphere due to inhibitory effects  
269 on decay<sup>24</sup>. All of these changes will be compounded by changes in hydrology, which will  
270 also affect overall peatland functioning. None of these potential changes have been taken into  
271 account in our projections of the future peatland carbon sink. Finally, human impact on the



272 peatland carbon store is still likely to be the most important determinant of global peatland  
273 carbon balance over the next century. Ongoing destruction of tropical peatlands is the largest  
274 contributor at present and at current rates, the losses from this source outweigh carbon  
275 sequestration rates in natural peatlands<sup>25,26</sup>. Whilst our results are reassuring in showing that  
276 the natural peatland C sink will likely increase in future, reducing anthropogenic release of  
277 peatland carbon is the highest priority in mitigation of peatland impacts on climate change.

278

### 279 **Corresponding Authors**

280 Angela Gallego-Sala and Dan Charman

281

### 282 **Acknowledgements**

283 The work presented in this article was funded by the Natural Environment Research Council  
284 (NERC standard grant number NE/I012915/1) to D.J.C., A.G.S., I.C.P., S.P. and P.F.,  
285 supported by NERC Radiocarbon Allocation 1681.1012. The work and ideas in this article  
286 have also been supported by PAGES funding, as part of C-PEAT. CDJ was supported by the  
287 Joint UK DECC/Defra Met Office Hadley Centre Climate Programme (GA01101). This  
288 research is also a contribution to the AXA Chair Programme in Biosphere and Climate  
289 Impacts and the Imperial College initiative on Grand Challenges in Ecosystems and the  
290 Environment. This research was also supported by a grant from the National Science Centre,  
291 Poland 2015/17/B/ST10/01656. We wish to thank Dale Vitt, Jukka Alm, Ilka E. Bauer,  
292 Nicole Rausch, Veronique Beaulieu-Audy, Louis Tremblay, Steve Pratte, Alex Lamarre,  
293 David Anderson and Alex Ireland for contributing data to this compilation. We are also  
294 grateful to Steve Frothingham for suggestions on different moisture indexes and to Alex Whittle  
295 and Fiona Dearden for their work in the Exeter laboratories.

296

### 297 **Author Contributions**

298 A.G.S. carried out analysis and interpretation of the data and wrote the first draft of the paper.  
299 D.J.C. supervised the project and contributed to experimental design, interpretation of results,  
300 and the final draft. S.B. carried out the statistical and spatial analysis of the data and contributed  
301 to the design of the final figures. S.M. was responsible for new radiocarbon analyses. Z.Y.  
302 provided the peatland map used in the modelling and contributed data and material. C.J.  
303 provided climate and gross primary productivity (GPP) data. L.O. carried out the age-depth  
304 models for all cores. All authors contributed either data or material to be analysed in the

305 Geography laboratories at the University of Exeter. All authors contributed to the preparation  
306 of the final paper.

307

### 308 **Additional Information**

309 The authors declare no competing financial interest.

310

### 311 **Figure captions**

312

313 Figure 1: Distribution of sampling sites in geographical space. Note that a single point may  
314 represent more than one site. (a) Locations of sites shown as either high-resolution records  
315 (white circles) or low-resolution records (black circles). (b) Distribution of fen (nutrient rich,  
316 green circle) and bog (nutrient poor, blue circle) or mixed (yellow circles) study sites. (c)  
317 Distribution of the mean annual carbon accumulation rate during the last millennium ( $\text{gC m}^{-2}$   
318  $\text{yr}^{-1}$ ) for all sites. Light yellow represents the lowest range of mean annual C accumulation (0-  
319  $10 \text{ gC m}^{-2} \text{ yr}^{-1}$ ) while dark brown represents the highest range ( $50\text{-}60 \text{ gC m}^{-2} \text{ yr}^{-1}$ ). Colours in  
320 between these two shades represent intermediate ranges, separated in  $10 \text{ gC m}^{-2} \text{ yr}^{-1}$  intervals.  
321

322 Figure 2: Controls on peat accumulation rate. Mean annual accumulation over the last 1000  
323 years at each site compared to a) cumulative annual photosynthetically active radiation (PAR0)  
324 b) latitude (degrees North are represented by positive numbers and degrees South by negative  
325 numbers) c) annual growing degree-days above  $0^\circ\text{C}$  (GDD0) and d) the ratio of precipitation  
326 over equilibrium evapotranspiration (moisture index, MI). Bog and fen sites (see Figure 1a and  
327 supplementary Table 1) are shown in blue and green respectively, and separate regressions  
328 have been calculated for each site type for PAR0 ( $R^2$  is shown on the graph). The grey line is  
329 the overall regression for all peat types. The regression for GDD0 yielded a much lower  $R^2$   
330 (only shown for all peat types). Errors represent uncertainty in carbon accumulation rates  
331 stemming from the age depth model errors (95 percentile range).  
332

333 Figure 3: Spatial analysis of the overall carbon sink. (a) Gridded spatial distribution of the  
334 annual carbon sink based on kriging of observations over the last millennium. Values have  
335 been kriged over a present-day peatland distribution map<sup>4</sup>. (b) Gridded spatial distribution of  
336 the annual carbon sink based on modelling of carbon accumulation for the last millennium  
337 calculated using the statistical relationship between the annual carbon sink and PAR0 (c)  
338 Difference between (a) and (b), negative values in red mean an overestimation of the sink  
339 using the statistically modelled data when compared with the observations, positive values in  
340 blue mean an underestimation of the sink by the model. Note: OK = Observation kriging. RK  
341 = Regression kriging  
342

343 Figure 4: Projected anomalies (future – historic) of annual carbon accumulation rates for  
344 three time periods: a) 2040-2060 b) 2080-2100, c) 2180-2200 and d) 2280-2300, based on  
345 PAR0 derived from climate data outputs from the Hadley Centre climate model. The climate  
346 runs chosen reflect the two end-member representative concentration pathways detailed in the  
347 IPCC Fifth Assessment Report<sup>31</sup>: 1) RCP2.5 and 2) RCP8.5.  
348

### 349 **References**

- 350 1 Friedlingstein, P., Cox, P., Betts, R., Bopp, L., von Bloh, W., Brovkin, V., Cadule,  
351 P., Doney, S., Eby, M. Fung, I., Bala, G., John, J., Jones, C., Joos, F., Kato, T.,  
352 Kawamiya, M., Knorr, W., Lindsay, K., Matthews, H.D., Raddatz, T., Rayner, P.,  
353 Reick, C., Roeckner, E., Schnitzler, K.-G., Schnur, R., Strassmann, K., Weaver,  
354 A.J., Yoshikawa, C. and Zeng, N. Climate-Carbon cycle feedback analysis: results  
355 from the C<sup>4</sup>MIP Model Intercomparison. *Journal of climate* **19** 3337-3353 (2006).
- 356 2 Gregory, J.M., Jones, C.D., Cadule, P. and Friedlingstein, P. Quantifying Carbon  
357 Cycle Feedbacks. *Journal of Climate* **22** 5232-5250 (2009).
- 358 3 Matthews, H. D., Eby, M., Ewen, T., Friedlingstein, P. and Hawkins, B.J. What  
359 determines the magnitude of carbon cycle-climate feedbacks? *Global*  
360 *Biogeochemical Cycles* **21** 12 (2007).
- 361 4 Yu, Z.C., Loisel, J., Brosseau, D.P., Beilman, D.W., Hunt, S.J. Global peatland  
362 dynamics since the Last Glacial Maximum. *Geophysical Research Letters*, **37**  
363 L13402 (2010)
- 364 5 Spahni, R., Joos, F., Stocker, B.D., Steinacher, M. and Yu, Z.C. Transient  
365 simulations of the carbon and nitrogen dynamics in northern peatlands: from the  
366 Last Glacial Maximum to the 21<sup>st</sup> century. *Climate of the Past* **9** 1287-1308 (2013)
- 367 6 Chaudhary, N., Miller, P. A., and Smith, B.: Modelling Holocene peatland  
368 dynamics with an individual-based dynamic vegetation model, *Biogeosciences*, **14**,  
369 2571-2596 (2017).
- 370 7 Ise, T., Dunn, A.L., Wofsy, S.C. and Moorcroft, P.R. High sensitivity of peat  
371 decomposition to climate change through water-table feedback. *Nature Geoscience*  
372 **1** 763-766 (2008)
- 373 8 Dorrepaal, E., Toet, S., van Logtestijn, R.S.P., Swart, E., van de Weg, M.J.,  
374 Callaghan, T.V. and Aerts, R. Carbon respiration from subsurface peat accelerated  
375 by climate warming in the subarctic. *Nature* **460** 616-619 (2009)
- 376 9 Wilson, R. M., Hopple, A. M., Tfaily, M. M., Sebestyen, S. D., Schadt, C. W.,  
377 Pfeifer-Meister, L., Medvedeff, C., McFarlane, K. J., Kostka, J. E., Kolton, M.,  
378 Kolka, R.K., Kluber, L. A., Keller, J. K., Guilderson, T. P., Griffiths, N. A.,  
379 Chanton, J. P., Bridgman, S. D. and Hanson, P. J. Stability of peatland carbon to  
380 rising temperatures. *Nature Communications* **7** 13723 (2011)
- 381 10 Blodau, C., Siems, M. and Beer, J. Experimental burial inhibits methanogenesis  
382 and anaerobic decomposition in water-saturated peats. *Environmental Science and*  
383 *Technology* **45** 9984-9989 (2011)

- 384 11 Loisel, J., Yu, Z., Beilman D.W., Camill, P., Alm, J., Amesbury, M.A., Anderson,  
385 D., Andersson, S., Bochicchio, C., Barber, K., Belyea, L.R., Bunbury, J.,  
386 Chambers, F.M. Charman, D.J., De Vleeschouwer, F., Fiałkiewicz-Kozieł, B.,  
387 Finkelstein, S.A., Gałka, M., Garneau, M., Hammarlund, D., Hinchcliffe, W.,  
388 Holmquist, J., Hughes, P., Jones, M.C., Klein, E.S., Kokfelt, U., Korhola, A.,  
389 Kuhry, P., Lamarre, A., Lamentowicz, M., Large, D., Lavoie, M., MacDonald, G.,  
390 Magnan, G., Mäkilä, M. Mallon, G., Mathijssen, P., Mauquoy, D., McCarroll, J.,  
391 Moore, T.R., Nichols J., O'Reilly, B., Oksanen, P., Packalen, M., Peteet, D.,  
392 Richard, P.J.H., Robinson, S., Ronkainen, T., Rundgren, M., Britta, A., Sannel, K.,  
393 Tarnocai, C., Thom, T., Tuittila, E.-S., Turetsky, M., Väliranta, M., van der  
394 Linden, M., van Geel, B., van Bellen, S., Vitt, D., Zhao, Y., and Zhou W. A  
395 database and synthesis of northern peatland soil properties and Holocene carbon  
396 and nitrogen accumulation. *The Holocene* **24** (9) 1028-1042 (2014).
- 397 12 Charman, D. J., Beilman, D. W., Blaauw, M., Booth, R. K., Brewer, S., Chambers,  
398 F. M., Christen, J. A., Gallego-Sala, A. V., Harrison, S.P., Hughes P.D.M., Jackson  
399 S.T., Korhola A., Mauquoy D., Mitchell F.J.G., Prentice I.C., van der Linden M.,  
400 De Vleeschouwer F., Yu Z.C., Alm J., Bauer I.E., Corish Y.M.C., Garneau M.,  
401 Hohl V., Y. Huang, E. Karofeld, G. Le Roux, J. Loisel, R. Moschen, Nichols J.E.,  
402 Nieminen T. M., MacDonald G.M., Phadtare N.R., Rausch N., Sillasoo Ü.,  
403 Swindles G.T., Tuittila E.-S., Ukonmaanaho L., Väliranta M., van Bellen S., van  
404 Geel B., Vitt D.H. and Zhao, Y. Climate-related changes in peatland carbon  
405 accumulation during the last millennium. *Biogeosciences* **10** 929–944 (2013).
- 406 13 Yu, Z. Holocene carbon flux histories of the world's peatlands: Global carbon  
407 cycle implications. *Holocene* **21** (5) 761-774 (2010).
- 408 14 Dargie, G.C., Lewis, S. L., Lawson, I.T., Mitchard E.T.A., Page, S.E., Bocko,  
409 Y.E., and Ifo S.A. Age, extent and carbon storage of the central Congo Basin  
410 peatland complex. *Nature* **542**, 86-90 (2017).
- 411 15 Michaletz, S.T., Cheng, D., Kerkhoff, A.J. & Enquist, B.J. Convergence of  
412 terrestrial plant production across global climate gradients. *Nature* **512** 39–43  
413 (2014).
- 414 16 Wang, H., Prentice, I. C., Keenan, T. F., Davis, T. W., Wright, I. J., Cornwell, W.  
415 K., Evans, B. J. & Peng, C. Towards a universal model for carbon dioxide uptake  
416 by plants. *Nature Plants* **3** 734–741 (2017).

- 417 17 Jones C, Robertson E, Arora V, Friedlingstein P, Shevliakova E, Bopp L, Brovkin  
418 V, Hajima T, Kato E, Kawamiya M. Twenty-first-century compatible CO<sub>2</sub>  
419 emissions and airborne fraction simulated by CMIP5 Earth System models under  
420 four representative concentration pathways. *Journal of Climate* **26**(13): 4398-4413,  
421 (2013).
- 422 18 Gorham E. Northern peatlands: Role in the carbon cycle and probable responses to  
423 climatic warming. *Ecological Applications* **1** 182–195 (1991).
- 424 19 Korhola, A., Alm, J., Tolonen, K., Turunen, J. & Jungner, H. Three-dimensional  
425 reconstruction of carbon accumulation and CH<sub>4</sub> emission during nine millenia in a  
426 raised mire. *Journal of Quaternary Science*, **11**, 161-165 (1996).
- 427 20 Väiliranta, M., Salojärvi, N., Vuorsalo, A., Juutinen, S., Korhola, A., Luoto, M.,  
428 Tuittila, E.-S. Holocene fen-bog transitions, current status in Finland and future  
429 perspectives. *The Holocene* **27**(5): 752-764 (2016).
- 430 21 Cooper, M. D.A., Estop-Aragonés, C., Fisher, J. P., Thierry, A., Garnett, M. H.,  
431 Charman, D. J., Murton, J. B., Phoenix, G. K., Treharne, R., Kokelj, S. V., Wolfe,  
432 S. A., Lewkowicz, A. G., Williams, M., and Hartley, I. P. Limited contribution of  
433 permafrost carbon to methane release from thawing peatlands. *Nature Climate*  
434 *Change*, **7**, 507-511 (2017).
- 435 22 Jones, M. C., Harden, J., O'Donnell, J., Manies, K., Jorgenson, T., Treat, C. and  
436 Ewing, S. Rapid carbon loss and slow recovery following permafrost thaw in  
437 boreal peatlands. *Global Change Biology* **23** 1109–1127 (2017).
- 438 23 Ott, C.A. and Chimner, R.A. Long-term peat accumulation in temperate forested  
439 peatlands (*Thuja occidentalis* swamps) in the Great Lakes region of North  
440 America. *Mires and Peat* **18** 1–9 (2016).
- 441 24 Wang, H., Richardson, C. J. and Ho, M. Dual controls on carbon loss during  
442 drought in peatlands. *Nature Climate Change* **5** 584-588 (2015).
- 443 25 Page, S. E., Siegert F., Rieley J.O., Boehm H.D., Jaya A. and Limin S. The amount  
444 of carbon released from peat and forest fires in Indonesia during 1997. *Nature* **420**  
445 61–65 (2002).
- 446 26 Moore, S., Evans, C. D.; Page, S. E.; Garnett, M. H.; Jones, T. G.; Freeman, C.;  
447 Hooijer, A., Wiltshire, A. J., Limin, S. H. and Gauci, V. Deep instability of  
448 deforested tropical peatlands revealed by fluvial organic carbon fluxes. *Nature* **493**  
449 660-663 (2013).
- 450

451

## 452 **Methods**

453 Carbon accumulation estimates. Mean annual carbon accumulation over the last millennium  
454 was estimated for 294 peatland sites (Table SIT1). In line with climate modelling studies, we  
455 use the term ‘last millennium’ to refer to the pre-industrial millennium between AD 850-1850).  
456 The total carbon accumulated over this period was calculated for all sites in Table SI1 by using  
457 a flexible Bayesian approach that incorporated estimates of age and minimum and maximum  
458 accumulation rates<sup>12</sup>. A number of sites were previously published (Reference 12 and  
459 references therein), but we added over 200 sites to the database from new field coring, as well  
460 as additional analysis for bulk density, carbon and radiocarbon dating from a range of existing  
461 samples held in laboratories around the world to bring the data to comparable standards. Age  
462 models were constructed from at least 2 radiocarbon dates (low resolution sites) or more than  
463 4 radiocarbon dates (high resolution sites) (see Table SI1 for details). For each of these records,  
464 bulk density was measured on contiguous samples. Carbon content was calculated based on  
465 either elemental carbon measurements or loss-on-ignition, when this was the case, loss-on-  
466 ignition was converted to total carbon assuming 50% of organic matter is carbon<sup>27</sup>.

467 The fen (minerotrophic or high nutrient, including poor fens) and bog (ombrotrophic or low  
468 nutrient) classification (Figure 1b) is a simplification and more information relating to each  
469 individual record is given in the supporting information (SI) section (Table SIT1). There are  
470 212 bogs versus 82 fens (which include 5 mixed sites).

471 We analysed the relationship between total carbon accumulation and a wide range of  
472 different climate parameters, including seasonal and mean annual temperature, precipitation  
473 and moisture balance indices (Figures 1d and SI1). Climate parameters were calculated using  
474 the CRU 0.5° gridded climatology for 1961-1990 (CRU CL1.0)<sup>28</sup>.

475 Modern day PAR0 and MI calculations. PeatStash<sup>29</sup> was used to calculate the accumulated  
476 PAR0 by summing the daily PAR0 over the growing season (days above freezing) for each  
477 peatland grid cell. The daily PAR0 is obtained by integrating the instantaneous PAR between  
478 sunrise and sunset. The seasonal accumulated PAR0 depends on latitude and cloudiness, and  
479 indirectly on temperature, because temperature determines the length of the growing season,  
480 i.e. which days are included in the seasonal accumulated PAR0 calculation. The Moisture  
481 Index (MI) was calculated as  $P/Eq$ , where  $P$  is annual precipitation and  $Eq$  is annually  
482 integrated equilibrium evapotranspiration calculated from daily net radiation and  
483 temperature<sup>29</sup>.  $P$  and  $Eq$  were also derived from CRU CL1.0.

484

485 Statistical model. The statistically modelled data are based on a relationship between C  
486 accumulation ( $\text{g C m}^{-2} \text{ yr}^{-1}$ ) and PAR0 ( $\text{mol phot m}^{-2} \text{ yr}^{-1}$ ) ( $R^2 = 0.25$ ,  $F_{2,292} = 49.35$ , p-value =  
487  $2.5 \times 10^{-19}$ ) as follows (Figure SI2, Table SI2):

488

$$489 \log_{10} C = 0.3 + 0.0003 \times PAR0 - 1.6 \times 10^{-8} \times PAR0^2 \quad (1)$$

490

491 This function is used when deriving a spatially explicit estimate of net carbon uptake using  
492 modern-day gridded PAR0 values (Figure 3b). The general trend is for the model to over-  
493 estimate the peatland carbon sink at high latitudes and underestimate it at low latitudes, when  
494 compared to the spatially interpolated data (Figure 3c). However, this is not uniform and the  
495 spatially interpolated data and the statistically derived model results compare well in areas of  
496 Eastern Siberia, China, Europe, southern North America, the tropical and Andean regions in  
497 South America and certain areas of central Africa. There is less congruence between spatially  
498 interpolated and statistically modelled estimates in areas where observations are lacking.

499

500 Spatial interpolation. To model the variation in spatial data, we use the model-based  
501 geostatistical approach described by Diggle and Riberio<sup>30</sup>, which decomposes the variation in  
502 a spatially distributed variable as follows:

503

$$504 Y(x) = \mu(x) + S(x) + \epsilon \quad (2)$$

505

506 where

507

- x is a spatial location; the coring sites
- Y is the value of the variable of interest; the carbon accumulation rate
- $\mu(x)$  is the mean field component, either as a constant mean or modelled using  
510 covariates (i.e.  $\mu(x) = \beta X$ )
- S(x) is the spatially random error, described by two parameters, the range ( $\phi$ ), giving  
512 the limit of spatial dependency and variance ( $\sigma^2$ )
- $\epsilon$  is the residual non-spatial random error, described by its variance ( $\tau^2$ )

514

515 The spatially random error describes the spatial dependence and can be modelled using one  
516 of a set of positive definite spatial covariance functions, which describe the decay in

517 covariance over distance<sup>31</sup>. Prediction for a new location ( $x'$ ) then follows the classic kriging  
518 approach of estimating the mean field component ( $\mu(x)$ ) and the deviation ( $S(x)$ ) from this at  
519 the new location, based on the covariance of this latter term with nearby locations<sup>32</sup>. The  
520 residual non-spatial error ( $\epsilon$ ) is then estimated as the kriging variance, giving estimation  
521 error. An alternative to method of estimating interpolation uncertainty is by a sequential  
522 simulation approach. Here, the spatially random error is simulated as multiple Gaussian  
523 random fields<sup>32</sup>, constrained on the observations, and the range of outcomes provides as  
524 estimate of the non-spatial error. All spatial analysis was carried out in R 3.3.2 using the  
525 packages 'gstat'<sup>33</sup> and 'raster'<sup>34</sup>.

526

527 Gridding observed accumulation rates. In a first step, we grid the observed carbon  
528 accumulation rates to a  $0.5^\circ$  grid clipped to a peatland mask<sup>4</sup> using ordinary sequential  
529 simulation. The mean field ( $\mu(x)$ ) is taken as the mean of the log10 carbon accumulation rates.  
530 The spatially random error term ( $S(x)$ ) was modelled from the observations using an  
531 exponential covariance function. This was then used to produce 1000 random spatial fields,  
532 conditional on both the covariance function and the locations of the observations. These fields  
533 were added back to the mean field to produce 1000 simulated carbon accumulation values, with  
534 the final values reported as the mean at each grid point. Interpolation uncertainties were  
535 estimated as the 95% confidence interval around the mean.

536

537 Gridding accumulation rates using PAR0. Here, the constant mean field of the previous model  
538 was replaced with the model described in equation 1. This provides estimates of estimate  
539 variations in the spatial mean field of log10 carbon accumulation rates across the  $0.5^\circ$  peatland  
540 grid based on modern PAR0 values (see Table SI2 for statistical significance of the different  
541 models). As in the previous step, the spatial random error term was estimated by sequential  
542 simulation of the model residuals at the observations sites, producing 1000 random spatial  
543 fields of residuals, which were then added back to the interpolated mean field to yield the  
544 present time carbon accumulation rate for the grid cell. Final values reported are the mean of  
545 the 1000 mean plus residual values at each grid point. The non-spatial error is then given by  
546 the 95% confidence interval from the 1000 simulations.

547

548 Estimating the future carbon sink. A similar approach was taken for the estimated future carbon  
549 accumulation. The mean field was estimated using equation 1, based on PAR0 projections for



550 two representative concentration pathways RCP2.5 and RCP8.5<sup>35</sup>, using climate projections  
551 for the periods 2040-2060, 2080-2100 and 2180-2200, as well as the historical period (1990-  
552 2005)<sup>36,37</sup>. To avoid bias from the climate model, future estimates of PAR0 are calculated as  
553 the anomaly between future and historical PAR0, added to the modern observed PAR0 field.  
554 The interpolated residuals from the previous step were then added to these to give estimates of  
555 future carbon accumulation rate for each grid cell with uncertainty estimated as before. It is  
556 important to note that while this approach allows the spatial mean field to change as a function  
557 of projected PAR0, the spatially auto-correlated error term is assumed to remain constant.

558

#### 559 Data Availability

560 The data set generated and analysed during the current study are available in the  
561 supplementary information section of this article and from the corresponding authors on  
562 reasonable request.

#### 563 References (Methods Section)

564

- 565 27 Bol, R. A., Harkness, D. D., Huang, Y. and Howard, D. M. The influence of soil  
566 processes on carbon isotope distribution and turnover in the British Uplands.  
567 *European Journal of Soil Science* **50** 41-51 (1999).
- 568 28 New, M., Hulme, M. and Jones, P.D. Representing twentieth century space- time  
569 climate variability. Part 1: development of a 1961-90 mean monthly terrestrial  
570 climatology. *Journal of Climate* **12** 829-856 (1999).
- 571 29 Gallego-Sala, A. V. and Prentice, I. C. Blanket peat biome endangered by climate  
572 change. *Nature Climate Change* **3** 152–155 (2013).
- 573 30 Diggle, P. and Riberio Jr, P.J. *Model-based geostatistics*. Springer-Verlag, New  
574 York, USA, 232 pp. (2007).
- 575 31 Cressie, N. A. C. *Statistics for spatial data*. New York, John Wiley & Sons Inc.  
576 (1993).
- 577 32 Goovaerts, P. *Geostatistics for natural resources evaluation*. Oxford University  
578 Press, Oxford, UK. 483 pp. (1997).
- 579 33 Pebesma, E.J. Multivariable geostatistics in S: the gstat package. *Computers &*  
580 *Geosciences*, **30**: 683-691 (2004).
- 581 34 Robert J. H, and van Etten, J. *Raster: Geographic analysis and modeling with raster*  
582 *data*. R package version 2.5-8. (2016).

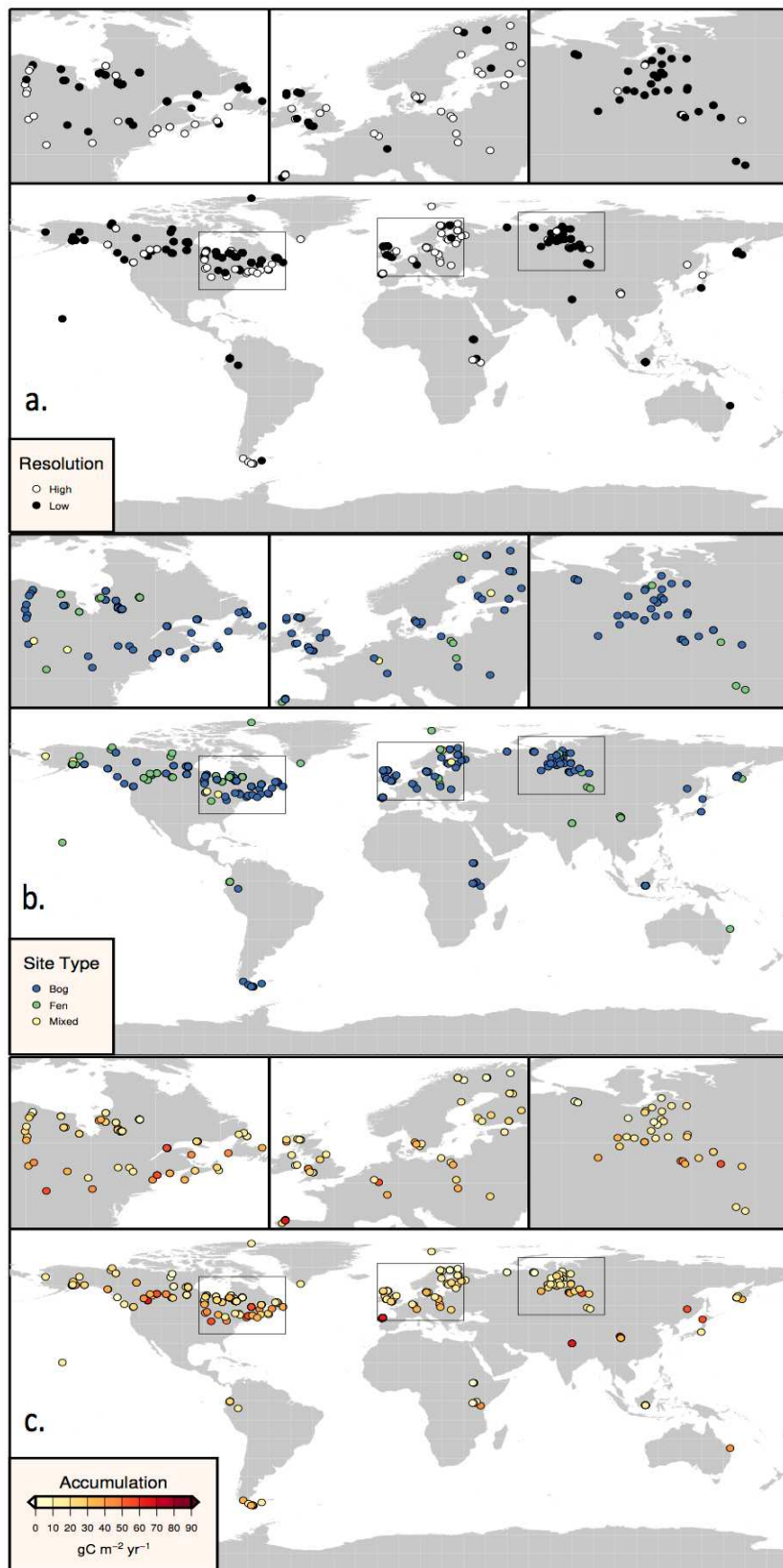
583 35 Intergovernmental Panel on Climate Change (IPCC) Fifth Assessment Report  
584 2014. Climate Change: Synthesis report (eds. Pachauri R.K. et al.) (2014)

585 36 Jones, C. D., Hughes, J. K., Bellouin, N., Hardiman, S. C., Jones, G. S., Knight, J.,  
586 Liddicoat, S., O'Connor, F. M., Andres, R. J., Bell, C., Boo, K.-O., Bozzo, A.,  
587 Butchart, N., Cadule, P., Corbin, K. D., Doutriaux-Boucher, M., Friedlingstein, P.,  
588 Gornall, J., Gray, L., Halloran, P. R., Hurtt, G., Ingram, W. J., Lamarque, J.-F.,  
589 Law, R. M., Meinshausen, M., Osprey, S., Palin, E. J., Parsons Chini, L., Raddatz,  
590 T., Sanderson, M. G., Sellar, A. A., Schurer, A., Valdes, P., Wood, N., Woodward,  
591 S., Yoshioka, M., and Zerroukat, M.: The HadGEM2-ES implementation of  
592 CMIP5 centennial simulations, *Geoscientific Model Development* **4** 543-570  
593 (2011).

594 37 Collins, W. J., Bellouin, N., Doutriaux-Boucher, M., Gedney, N., Halloran, P.,  
595 Hinton, T., Hughes, J., Jones, C. D., Joshi, M., Liddicoat, S., Martin, G., O'Connor,  
596 F., Rae, J., Senior, C., Sitch, S., Totterdell, I., Wiltshire, A., and Woodward, S.:  
597 Development and evaluation of an Earth-System model – HadGEM2,  
598 *Geoscientific Model Development* **4** 1051-1075 (2011).

599  
600  
601

602 FIGURE 1  
603



604  
605

